Selection rules for the tip-splitting instability

A. Pereira*
Centre de Recherche Paul Pascal, CNRS, Avenue Schweitzer, 33600 Pessac, France

J. Elezgaray†
IECB, 16 Avenue Pey-Berland, 33607 Pessac, France

(Received 24 June 2003; revised manuscript received 20 October 2003; published 23 February 2004)

The local destabilization of a Saffman-Taylor viscous finger occurs by a splitting of its tip and results in the formation of two branches separated by a fjord. The accumulation of such instabilities leads to complex patterns. In this paper we present a detailed analysis of a dynamical model that accounts for the selection of both the width and the orientation of the fjords growing in a wedge of angle θ_0. It is shown that the selection rules have a dynamical origin and are related to the existence of attracting sets that disappear in the absence of surface tension. We also infer the existence of a critical angle $\theta_c = 60°$ such that if $\theta_0 < \theta_c$, the symmetric tip-splitting becomes unstable.

DOI: 10.1103/PhysRevE.69.026301 PACS number(s): 47.20.−k, 47.15.Hg, 47.20.Hw, 68.05.−n

I. INTRODUCTION

The displacement of a viscous fluid by a less viscous one in a quasi-two-dimensional Hele-Shaw cell [1] is among the most studied problems in interfacial pattern formation [2]. A rich variety of patterns is observed in this configuration, whereas the opposite situation (the more viscous fluid is pushing the less viscous one) always leads to a stable flat interface between the two. After more than one decade of work in this field, most questions concerning the stable regime observed in the channel geometry are now well understood. Historically, the study of the so-called selection rules that govern the shape of the fingers observed in this configuration is at the origin of the wide interest raised by this system. On the contrary, in radial geometry, there is no indication that a steady state is ever achieved. In this second configuration, the less viscous fluid initially forms a bubble (almost a circular interface), but as more fluid is injected, the interface becomes unstable, developing fingers or petals that, contrarily to the channel case, are eventually destabilized by the so-called tip-splitting instability. The accumulation of such instabilities leads to a ramified, fractal structure, similar in many aspects to that observed in diffusion-limited aggregation (DLA).

Most questions concerning the unstable regime remain still unsolved. One of the most striking is the existence of a well defined fractal dimension D_f. Several theories [3–6] exist that predict values $D_f \sim 1.7$. Recently, it has been pointed out [7] that viscous fingering and DLA do not belong to the same universality class (thus, do not have the same fractal dimension), contrary to a well established consensus. An experimental confirmation of this fact remains still difficult. The fractal structures observed in viscous fingering are made up of wedge-shaped building blocks [8]. Roughly speaking, each finger grows in a wedge formed by its two neighbors. The regions of fluid that separate two neighbor fingers are called fjords in the following. There is experimental evidence [8] for the existence of a critical angle θ_c: when the wedge angle $\theta_0 < \theta_c$, there is competition between the two fingers formed in the tip-splitting and the result will be a side-branched finger. Instead, when $\theta_0 > \theta_c$, the two fingers coexist. Motivated by the importance of the wedge geometry, Combescot *et al.* [9] showed by a careful study of the selection mechanisms in this geometry that both the angular width and the radius at which tip splitting occurs are selected by surface tension. However, this analysis relies on the assumption that the interface is self-similar, a fact well verified in the early stages of the growth but certainly wrong in the vicinity or the subsequent development of the instability. Sarkar [3] used this idea to estimate D_f by counting the number of tip splittings along the growth. This appears to be the simplest mean field theory accounting for the value of D_f. It contains a unique free parameter β, related to θ_c and the selected width of the fjords. A theoretical prediction for β is given below.

The studies mentioned so far boil down to the solution of a time independent integral equation describing the shape of the interface. A different line of thought started with the work of Tanveer [10], which rather focused on the singular character of the surface tension term which is at the origin of the selection rules. One of the most striking results obtained in this direction is the fact that the addition of a small surface tension may induce strong perturbations even in $O(1)$ time. This is obviously difficult to monitor experimentally but has been verified numerically [11]. It is interesting to note that the connection between the singular character of surface tension and the existence of selection rules has been criticized by some authors [12] who suggested that the latter are a simple dynamical effect. Contrary to the integral equation method, Tanveer's analysis is applicable in time dependent situations and relies on the notion of singularity of the conformal mapping. This notion will be explained in detail in the following section.

The aim of this paper is to introduce of a model that is able to handle tip-splitting and non-self-similar solutions in a

*Electronic address: pereira@crpp-bordeaux.cnrs.fr
†Electronic address:
j.elezgaray@iecb-polytechnique.u-bordeaux.fr

simple and unified way. Our initial motivation comes from the experimental observations made by Lajeunesse and Couder [8] that the form of the fjord separating any two fingers formed in a tip splitting can be understood using a simple geometrical construction. The middle point of each fjord describes a trajectory that in Ref. [8] was approximated by that of a perturbation advected by the selected zero surface tension solution [13] (this construction will be called in the following the ''normal rule''). This argument was also generalized to secondary tip-splittings, using the notion of virtual walls. They also observed a critical angle $\theta_c \sim 70°$, significantly smaller than the value predicted in Ref. [4]. This appears to be the first unambiguous experimental set of data clearly showing that the increasing complexity of the patterns observed in the unstable regime corresponds to a hierarchy of virtual cells of various sizes. Similar results have been obtained by Arneodo *et al.* for DLA clusters [14] and quasi-two-dimensional electrodeposition clusters.

The rest of the paper is organized as follows. In the following section, we introduce the notion of the conformal mapping and the associated singularities. This will be used to derive an approximate dynamical model that we study in the third section. Next, we consider the phase portraits of this dynamical system and show the existence of attracting sets and relate them to selection rules. A final section will draw some conclusions and perspectives.

II. CONFORMAL MAPPINGS

The basic difficulty in studying the evolution of the fluid interface in the classical Saffman-Taylor experiment is the fact that the normal velocity at each point of the interface is given by the normal gradient of the pressure p in the more viscous fluid, which in turn satisfies the Laplace equation $\Delta p = 0$, provided the Darcy approximation is assumed. The solution of this equation is not trivial, even numerically. A convenient way to circumvent this problem is the use of a change of variables, the so-called conformal mapping $f(\xi,t)$, which maps the interior of the unit circle $|\xi| \leqslant 1$ onto the domain occupied by the more viscous fluid. Furthermore, the interface at time t, $\Gamma(t)$, appears now to be the image of the unit circle: for each point $z \in \Gamma(t)$, there exists an angle $\theta = \theta(z,t)$ such that $z = f(e^{i\theta},t)$. The main interest of such a mapping is that the transformed Laplace equation in the new ξ coordinates is again the Laplace equation. This is strictly due to the fact that $f(\xi,t)$ is conformal, which is analytic and of nonzero derivative, in the interior of the unit disc. Furthermore, the solution of the Laplace equation in the interior of the unit disk is explicitly known through the use of the Poisson kernel. Let us now be more precise. The conformal mapping will be written as

$$f(\xi,t) = \frac{a(t)}{\xi} + k(\xi,t), \tag{1}$$

where $a(t)$ can be chosen to be positive and $k(\xi,t)$ is an analytic function in the whole disk, including 0. In the above equation, the first term corresponds to a circle of radius $a(t)$, perturbed by the deformation $k(\xi,t)$. Let $\Phi(\xi,t)$ be the complex velocity potential. It can be shown [10] that

$$\Phi(\xi,t) = -\frac{Q}{2\pi}\ln \xi + \omega(\xi,t), \tag{2}$$

where ω is an analytic function in $|\xi| < 1$ such that

$$\mathrm{Re}\,\omega = -T\frac{1}{|\partial_\xi f|}\mathrm{Re}\left(1 + \frac{\partial_\xi^2 f}{\partial_\xi f}\right) \quad \text{when } |\xi| = 1. \tag{3}$$

Here, Q stands for the net flux imposed at infinity and T is the surface tension coefficient, such that the pressure drop $[p]$ at the interface is $[p] = T\kappa$, κ being the local curvature (this is the Laplace condition).

The evolution equation $\partial_t f = \mathcal{F}(f)$ [10,15] of the conformal mapping is just a translation of the evolution equation of the interface $v_n = \partial_n p$, where v_n is the normal velocity of the interface and $\partial_n p$ is the normal gradient of the pressure. It has been shown [10] that

$$\mathcal{F}(f(\xi,t)) = \xi \partial_\xi f I(\xi), \tag{4}$$

where $I(\xi,t)$ is the normal velocity at the point of the interface corresponding to ξ:

$$I(\xi) = \frac{1}{2\pi}\int_{|\xi'|=1} \frac{d\xi'}{i\xi'}\frac{\xi+\xi'}{\xi'-\xi}\frac{1}{|\partial_{\xi'} f|^2} \times \left(-\frac{Q}{2\pi} + \mathrm{Re}[\xi' \partial_{\xi'}\omega(\xi')]\right). \tag{5}$$

This expression highlights the two contributions of the velocity at the interface, the first one coming from the boundary conditions at infinity (the net flux is fixed to be equal to Q) and the other one being related to the Laplace condition. The expression of $\omega(\xi)$ involves the evaluation of an integral (Poisson) kernel, and is difficult to compute explicitly due to the presence of the term $1/|\partial_\xi f|$:

$$\omega(\xi) = -\frac{T}{2\pi}\int_{|\xi'|=1} \frac{d\xi'}{i\xi'}\frac{\xi+\xi'}{\xi'-\xi}\frac{1}{|\partial_{\xi'} f|}\mathrm{Re}\left(1 + \xi'\frac{\partial_{\xi'}^2 f}{\partial_{\xi'} f}\right). \tag{6}$$

In Ref. [15], $\omega(\xi)$ was actually computed through a numerical evaluation [16] of the integral in Eq. (6). This renders the resulting equations difficult to study analytically (and even numerically).

The mapping $f(\xi,t)$ is analytic in $0 < |\xi| < 1$ but may display singularities outside. In the absence of surface tension, the number and nature (local exponent) of each singularity are conserved; namely, if N singularities are present in the initial condition, typically the asymptotic interface will display N deformations (protrusions in the case of poles in f_ξ, cusps in the case of zeros of f_ξ) that correspond to the approach of these singularities to the unit circle. The situation is rather different in the presence of surface tension [10]. Several authors have already shown that the effect of surface tension can be dramatic on the number (creation of daughter

singularities with exponent $-4/3$) and the motion of these singularities. It has also been shown [11] that arbitrarily small values of surface tension may induce significant perturbations of the interface in $O(1)$ time. To give a physical description of this creation process, it is useful to refer to the situation created by the introduction of nonlinearities in a linear equation, such as the simplest linear diffusion equation. It is well known that in the linear case, any finite set of Fourier modes is an exact solution of this equation (with periodic boundary conditions), whereas the introduction of any nonlinearity induces the creation of small scale modes that have to be taken into account. Similarly, in the absence of surface tension, any finite set of logarithmic singularities is an exact solution of Eq. (4) [17], even though the equations are nonlinear. This is due to the existence of conservation laws [18]. The addition of surface tension induces the creation of daughter singularities, with exponent $-4/3$ [10]. Clearly, these new singularities are responsible for the surface induced tip-splitting process.

In the following, we consider a simple model of this complex process in which the singularities are strictly logarithmic:

$$f(\xi,t)=\frac{a(t)}{\xi}+\sum_{k=1}^{N}\sum_{l=0}^{s-1}c_k(t)e^{-2i\pi l/s}\ln[\xi-p_k(t)e^{2i\pi l/s}], \tag{7}$$

where s is a positive integer. In Ref. [15], it was shown that the restriction to logarithmic singularities is not a real limitation, because an accumulation of such singularities can approach arbitrarily close [19] a singularity of the form $(\xi-\xi_0)^{-4/3}$, as those expected in the present problem; namely, this boils down to the standard Padé approximation [19] of the function $\partial_\xi f$ by a rational function, as can be seen by differentiation of Eq. (7). In the following, we will adopt the following notation for this derivative:

$$\partial_\xi f(\xi,t)=A(t)\xi^{-2}\prod_k\frac{\xi^s-z_k(t)^s}{\xi^s-p_k(t)^s}, \tag{8}$$

where the z_k's (p_k's) are the zeros (poles) of $\partial_\xi f(\xi,t)$. Because $f(\xi,t)$ is conformal in $0<|\xi|<1$, we have $|z_k(t)|>1$ and $|p_k(t)|>1$. It is easy to see that

$$a(t)=-A(t)\prod_k\left[z_k^s(t)/p_k^s(t)\right] \tag{9}$$

and

$$c_k=(A/sp_k^{s+1})\left(\prod_j(p_k^s-z_j^s)\Big/\prod_{j\neq k}(p_k^s-p_j^s)\right). \tag{10}$$

In the following, we will note $p_k=(1+\rho_k)e^{i\phi_k}$, $z_k=(1+r_k)e^{i\theta_k}$. The position of the bottom of each fjord is $-Ae^{-i\phi_k}+c_k\ln(e^{i\phi_k}-p_k)$ (we have $z_k\approx p_k$ and $\rho_k\to 0$ when $t\to+\infty$), and its width is $\pi|c_k|$. This can be seen by inspecting the behavior of the logarithmic function in the vicinity of $\xi=e^{i\phi_k}$. For the sake of simplicity, let us consider the simplest case of a single singularity. It is possible to obtain the exact form of the bottom of the fjord in the limit $t\to+\infty$. In order to do so, let us introduce the function $\alpha:t\mapsto\alpha(t)$ that will be used as a parametrization of the interface. In order to get a finite limit as $t\to+\infty$, it is necessary to set $\alpha(t)=\gamma\rho_1(t)+\phi_1(t)$, where γ is a parameter. The asymptotic, shape of the fjords is then

$$\check{z}(\gamma)=\lim_{t\to+\infty}f(e^{i\alpha(t)},t), \tag{11}$$

where $\gamma\in\,]-\infty,+\infty[$. Taking into account the hypothesis on the asymptotic behavior of c_k and p_k, we get

$$\check{z}(\gamma)=z(1,\infty)+c_1(\infty)(\ln\sqrt{1+\gamma^2}-i\arctan\gamma), \tag{12}$$

where $z(1,\infty)$ is the position of the bottom of the fjord when $t\to+\infty$. This simple computation shows that the parametrization of the interface in the vicinity of the bottom of the fjords is closely related to the distance of the poles to the unit circle. The latter being asymptotically very small, this will be one of the main difficulties in the numerical implementation of the model.

III. THE DYNAMICAL MODEL

From the above considerations, it is clear that the form given by Eq. (7) is not an exact solution of the evolution equation (4). In the present case, this is due to the fact that the surface tension term induces singularities that are not present in Eq. (7). Following the approach in Ref. [15], the dynamics will be defined in such a way that the error

$$\mathcal{E}(t)=\int_{|\xi|=1}\left|\frac{d}{dt}\left(\frac{A(t)}{\xi^2}\prod_{k=1}^{N}\frac{\xi^s-z_k^s(t)}{\xi^s-p_k^s(t)}\right)-\partial_\xi\mathcal{F}(f(\xi,t))\right|^2 d\xi \tag{13}$$

is minimized. In other terms, at each time t, we choose the time derivatives of the variables A, z_k, and p_k in such a way that the average (on the unit circle) deviation between the physical dynamics and the dynamics of the model is minimized. One of the advantages of using the logarithmic approximation of the conformal mapping is that the minimization of $\mathcal{E}(t)$ can be done in an analytic way. If the evolution equation is written in the form $\partial_t\{\ln[\partial_\xi f(\xi,t)]\}=F(\xi,t)$, where $F(\xi,t)=\partial_\xi[\mathcal{F}(f(\xi,t))]/\partial_\xi f$:

$$F(\xi,t)=\left(1+\xi\frac{\partial_\xi^2 f(\xi,t)}{\partial_\xi f(\xi,t)}\right)I(\xi,t)+\xi\partial_\xi I(\xi,t), \tag{14}$$

the minimization yields the following linear system:

$$\sum_j\frac{s}{(z_i^*z_j)^s-1}\frac{\dot{z}_j}{z_j}-\sum_j\frac{s}{(z_i^*p_j)^s-1}\frac{\dot{p}_j}{p_j}=F(1/z_i^*)-F(0), \tag{15a}$$

$$\sum_j\frac{s}{(p_i^*z_j)^s-1}\frac{\dot{z}_j}{z_j}-\sum_j\frac{s}{(p_i^*p_j)^s-1}\frac{\dot{p}_j}{p_j}=F(1/p_i^*)-F(0), \tag{15b}$$

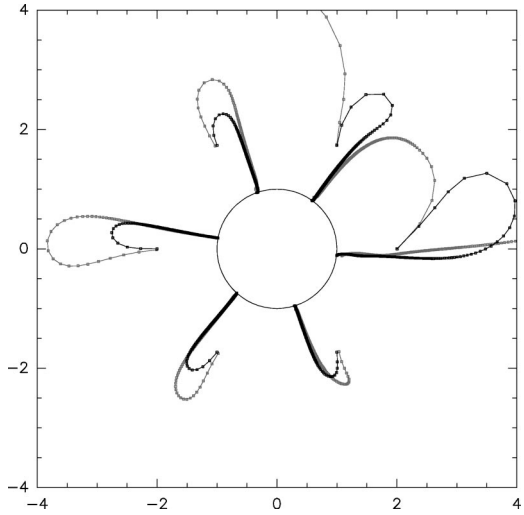

FIG. 1. A typical example of trajectories for the zeros (light line) and the poles (dark line) of $\partial_\xi f$ in the complex plane. The corresponding interfaces are represented in Fig. 2. First far from the unit circle, the couples of singularities approch a it at different speeds. For the sake of clarity, parts of the trajectory of the zero z_2 located near (1,1.5) at $t=0$ are not represented ($|z_2|>18$ at $t=1.5$).

together with the equation

$$\frac{\dot{A}}{A}=F(0)-s\left(\sum_j \frac{\dot{z}_j}{z_j}-\sum_j \frac{\dot{p}_j}{p_j}\right). \tag{15c}$$

In Ref. [15], it was shown that despite its simplicity this model can account for many aspects of the tip-splitting instability, and compares well to the interfaces obtained by a pseudospectral method [20]. Here, we show an example that illustrates the typical behavior of the singularity dynamics (Fig. 1) and the corresponding behavior for the interface (Fig. 2). Six couples of zeros and poles are present at $t=0$. In order to obtain an almost circular interface at $t=0$, $z_k \approx p_k, k=1,\ldots,6$. The trajectories of the singularities display most of the time a first short regime where the dynamics is quite rapid and some of the zeros and poles can get quite far from the unit circle, although eventually they become closer. Surprisingly, this regime does not have an analog in the physical space: the interface evolves smoothly and only in the second regime, when the poles get very close to the unit circle, there is a significant incidence on the shape of the interface and the fjords start to form. Notice also that the couples initially present are not necessarily those that form asymptotically. This should be compared to the asymptotic results shown by Tanveer, which imply that the daughter singularities are, at times $O(1)$, in a neighborhood of size $O(T^{1/3})$ around the singularity of the zero surface tension problem. Such a behavior is not immediately evident from our data. The difference is probably due to the fact that the value of the surface tension parameter we used here is not in the range of validity of the results in Ref. [10]. Let us also notice that the distance that the pole singularities move away from the unit disk decreases in our model (results not shown here) when T decreases. A detailed comparison of such a behavior against the perturbative calculations of Tanveer will be reported elsewhere.

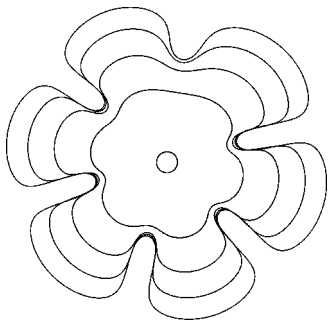

FIG. 2. Successive interfaces corresponding to the set of singularities of Fig. 1.

We have used three methods to evaluate the time derivatives of the dynamical model. The first method computes all the integrals appearing in the right-hand side (rhs) of Eq. (15a) and (15b) by direct discretization on the ξ variables, and the principal value integral needed to compute $\omega(\xi)$ is done using the fast Fourier transform [16]. Unfortunately, when the poles get close to the unit circle, this transform requires a huge number of points in order to approximate the almost singular functions in the integrand of $I(\xi)$ and the method becomes quickly unpractical. A second approach relies on the observation that

$$I(\xi,t)=-\frac{1}{2\pi}\int_{|\xi'|=1}\frac{d\xi'}{i\xi'}\frac{\xi'+\xi}{\xi'-\xi}\frac{v_n(\xi')}{|\partial_\xi f(\xi')|}, \tag{16}$$

where v_n is the normal velocity. In other words, once v_n is known on the interface, relation (16) provides the necessary information to compute the time derivatives of z_k, p_k, and A. Contrary to the first method, the discretization is done on the physical interface, and the recourse to the Fourier transform is not necessary. v_n can be computed using the methods in Ref. [20], although an appropriate parametrization of the interface is needed in order to get an efficient algorithm. The numerical details will be given elsewhere.

A third method was introduced in order to get further insight into the structure of the dynamical system (15) and provide a fully analytical approximation of the surface tension term, by the use of a Padé approximation [19] to $1/|\partial_\xi f|$. This is based on the identity (valid for $|\xi|=1$)

$$\frac{|\xi^s-p^s|}{|\xi^s-z^s|}=\sqrt{\frac{p^{*s}}{z^{*s}}}\sqrt{1+\frac{p^s-z^s}{z^s-\xi^s}}\sqrt{1+\frac{1/p^{*s}-1/z^{*s}}{1/z^{*s}-\xi^s}} \tag{17}$$

and the Padé approximation

$$\sqrt{1+z}=\lim_{P\to+\infty}\prod_{\alpha=1}^{P}\frac{\mu_\alpha(P)}{\nu_\alpha(P)}\frac{z-\nu_\alpha(P)}{z-\mu_\alpha(P)}, \tag{18}$$

where $\nu_\alpha(P)$ and $\mu_\alpha(P)$ belong to $]-\infty,-1[$. Using these expressions, it is straightforward to compute the approximation (for $|\xi|<1$)

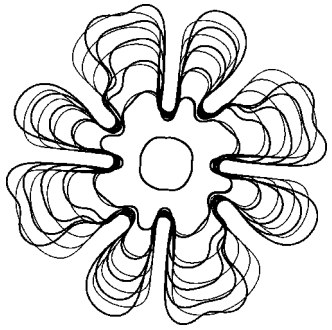

FIG. 3. Comparison between the interface obtained by the pseudospectral code (thick line) and that from the N-singularity model with $N=2$ and $s=4$ (thin line).

$$\omega(\xi)\approx\omega_0+\sum_k \frac{\omega_{1k}}{\xi^s-z_k^s}+\sum_k \frac{\omega_{2k}}{\xi^s-p_k^s}+\sum_{\alpha,k} \frac{\omega_{3\alpha,k}}{\xi^s-p_{\alpha,k}^s}, \tag{19}$$

with

$$p_{\alpha,k}^s=\frac{1+\mu_\alpha}{\mu_\alpha}z_k^s-\frac{1}{\mu_\alpha}p_k^s, \quad \alpha=1,\ldots,P, \tag{20}$$

where P is the order of the Padé approximation. Equation (19) defines how new singularities are added to the model: starting from the set of initial singularities z_k, p_k, those given by the interface itself, the inclusion of the curvature term creates automatically the $p_{\alpha,k}$ set. These new singularities are always located on the segment going from z_k to p_k. In order to reach the minimum of $\mathcal{E}(t)$, new singularities located at $p_{\alpha,k}$ should be added in turn as variables of the model. Here, we decide to limit the set of variables to the zeros z_k and poles p_k of the interface. However, in order to illustrate how increasing the number of singularities improves the approximation to the actual solution, we show in Figs. 3 and 4 the patterns obtained with, respectively, 4×2 and 4×3 couples of zero poles. The initial interface only has 4×2 couples of singularities that correspond to the 4×2 deeper fjords. The surface tension induces a secondary tip-splitting on the side of the thickest finger as can be seen on the interface corresponding to the ''true'' solution (thick line in Figs. 3 and 4). Adding four new couples of singularities

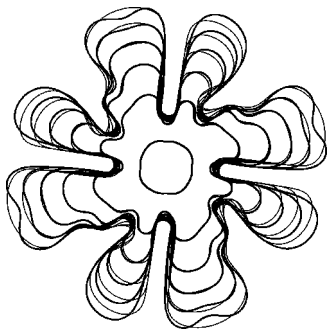

FIG. 4. Same as Fig. 3 but with $N=3$. The increase in the number of singularities gives a better approximation of the third tip splitting.

(Fig. 4) significantly improves the approximation. It is worth noting that the position of the third fjord is quite robust, a fact experimentally observed by Lajeunesse and Couder [8]. Actually, the four new singularities can be placed almost randomly (provided the zero-pole couple is far from the unit circle); they eventually converge to a well defined angular position. This will be partly explained below.

Using approximation (19), the evaluation of the rhs of Eq. (15) is straightforward. The resulting expression is somewhat lengthy and will be given elsewhere. We thus obtain a closed set of explicit evolution equations for (A,z_k,p_k) of the form

$$[\dot{A},\dot{z}_k,\dot{p}_k]=F_P(A,z_k,p_k), \tag{21}$$

where F_P is a vector of algebraic functions, dependent on the degree P. This Padé approximation will allow us to study in detail the whole phase portrait determining the singularity dynamics.

The general analysis of such a system is still difficult. We will rather study some generic situations. In order to mimic the experimental results of Ref. [8], we will first consider s symmetric solutions (s even, due to the zero-flux conditions at the walls), corresponding to viscous fingering in a wedge of angle $2\pi/s$ [21]. Under such conditions, the primary fjords, associated with the couple (z_1,p_1) are parallel to the walls of a wedge with angle $2\pi/s$ and the secondary fjords [corresponding to (z_2,p_2)] yield the first tip-splitting.

IV. ONE-SINGULARITY SYMMETRIC SOLUTIONS

In a real experiment, the interface between the two fluids is initially smooth, which means that at the very beginning, all the singularities are far from the unit circle and the $a(t)/\xi$ term is predominant. Because of the constant flux condition, $a(t)\sim|A(t)|\sim t^{1/2}$. As the growth proceeds, all the singularities approach the unit circle [10], but this approach is hierarchical, in the sense that only a limited number of singularities can be located at a certain distance from the unit disk.

In close analogy with previous studies [9], in Ref. [21] we studied the selection mechanism that fixes the value of the width of the primary fjords, i.e., the value $r_1(t)$ of the closest (primary) singularity. We give here a detailed presentation of this point.

When only one singularity is present, the system of equations (15) becomes

$$\frac{s}{(z^*z)^s-1}\frac{\dot{z}}{z}-\frac{s}{(z^*p)^s-1}\frac{\dot{p}}{p}=F(1/z^*)-F(0), \tag{22}$$

$$\frac{s}{(p^*z)^s-1}\frac{\dot{z}}{z}-\frac{s}{(p^*p)^s-1}\frac{\dot{p}}{p}=F(1/p^*)-F(0). \tag{23}$$

This system can be solved to yield

$$\left(1-\frac{(|p|^{2s}-1)(|z|^{2s}-1)}{|(pz^*)^s-1|^2}\right)\frac{\dot{z}}{z} = \frac{|z|^{2s}-1}{s}\left([F(1/z^*)-F(0)] - \frac{|p|^{2s}-1}{(z^*p)^s-1}[F(1/p^*)-F(0)]\right), \quad (24)$$

$$\left(1-\frac{(|p|^{2s}-1)(|z|^{2s}-1)}{|(p^*z)^s-1|^2}\right)\frac{\dot{p}}{p} = \frac{|p|^{2s}-1}{s}\left(\frac{|z|^{2s}-1}{(p^*z)^s-1}[F(1/z^*)-F(0)] - [F(1/p^*)-F(0)]\right). \quad (25)$$

From the equations above, it is clear that if z and p are initially real, they remain real for all times [in that case, $F(0)$, $F(1/z^*)$, and $F(1/p^*)$ are also real]. Furthermore, we have seen that the argument of a can be chosen to be independent of t ($\mathrm{Im}[F(0)]=0$) so that a is also real. Therefore, we just have to consider the variables a, r, and ρ.

In the limit $\rho\to 0$, Eqs. (24) and (25) become

$$\frac{\dot{r}}{1+r} = [1+O(\rho)][(1+r)^{2s}-1][F(1/z^*)-F(0)]/s - 2\rho[1+O(\rho)][(1+r)^s+1][F(1/p^*)-F(0)] \quad (26)$$

and

$$\frac{\dot{\rho}}{2\rho} = [1+O(\rho)][(1+r)^s+1][F(1/z^*)-F(0)] - [1+O(\rho)][F(1/p^*)-F(0)]. \quad (27)$$

At this point, it is convenient to separate in F the contribution due to the flux Q from that one due the surface tension T: $F=F_Q+F_T$. The F_Q term can be computed explicitly:

$$F_Q(0) = \frac{1}{|A|^2}\left(\prod_k \frac{p_k^s}{z_k^s} - \sum_k b_k\right)\frac{Q}{2\pi}, \quad (28)$$

$$F_Q(1/p_j^*) = \frac{-Q}{2\pi}\frac{1}{|A|^2} \times\left[\left(-1+\sum_k \frac{sp_j^{*s}(z_k^s-p_k^s)}{(1-z_k^s p_j^{*s})(1-p_k^s p_j^{*s})}\right) \times\left(\sum_k \frac{a_k}{z_k^s}\frac{1+z_k^s p_j^{*s}}{1-z_k^s p_j^{*s}}+c\right) - \sum_k \frac{2sp_j^{*s}a_k}{(1-z_k^s p_j^{*s})^2}\right], \quad (29)$$

and

$$F_Q(1/z_j^*) = \frac{-Q}{2\pi}\frac{1}{|A|^2}\left[\left(-1+\sum_k \frac{sz_j^{*s}(z_k^s-p_k^s)}{(1-z_k^s z_j^{*s})(1-p_k^s z_j^{*s})}\right) \times\left(\sum_k \frac{a_k}{z_k^s}\frac{1+z_k^s z_j^{*s}}{1-z_k^s z_j^{*s}}+c\right) - \sum_k \frac{2sz_j^{*s}a_k}{(1-z_k^s z_j^{*s})^2}\right], \quad (30)$$

which leads, in the limit $\rho\to 0$, to the following expressions:

$$F_Q(0) \sim \frac{Q}{2\pi}\frac{1}{|A|^2}\frac{2}{(1+r)^s[1+(1+r)^s]}, \quad (31)$$

$$F_Q(1/z^*)-F_Q(0) \sim \frac{Q}{2\pi}\frac{1}{|A|^2}\frac{-2}{[(1+r)^s+1]^2(1+r)^s}, \quad (32)$$

$$F_Q(1/p^*)-F_Q(0) \sim \frac{Q}{2\pi}\frac{1}{|A|^2}\frac{(s-2)(1+r)^s+2}{[(1+r)^{2s}-1](1+r)^s}. \quad (33)$$

On the other hand, in the limit $\rho\to 0$ and $r\to 0$, we find that

$$F_T(0) \sim T\alpha_0|A|^{-3}\rho^0 r^{-1}, \quad (34)$$

$$F_T(1/z^*)-F_T(0) \sim T\alpha_z|A|^{-3}\rho^0 r^{-3}, \quad (35)$$

$$F_T(1/p^*)-F_T(0) \sim -T\alpha_p|A|^{-3}\rho^{-1} r^{-2}, \quad (36)$$

where α_0, α_z, and α_p are positive constants.

When $T=0$, we get from relations (26), (27), (32), and (33)

$$\frac{\dot{r}}{1+r} = -\frac{Q}{2\pi}\frac{1}{|A|^2}\frac{2[(1+r)^s-1]}{s[(1+r)^s+1](1+r)^s}[1+O(\rho)]. \quad (37)$$

and

$$\frac{\dot{\rho}}{2\rho} = -\frac{Q}{2\pi}\frac{1}{|A|^2}\frac{s}{(1+r)^{2s}-1}[1+O(\rho)]. \quad (38)$$

From Eqs. (37) and (38), the asymptotic behavior of r and ρ in the limit $\rho\to 0$ and $r\to 0$ is

$$r \sim \frac{r_0}{\sqrt{t}}, \quad (39)$$

$$\rho \sim \rho_0 e^{-\sqrt{t}/r_0}. \quad (40)$$

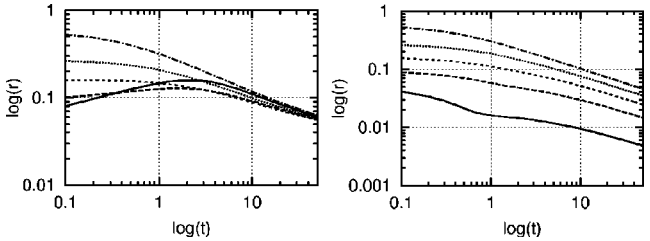

FIG. 5. Comparison of the behavior of $r(t)$ as $t\to+\infty$ when (a) $T>0$ (all the initial conditions converge to a unique solution) and (b) $T=0$.

Therefore, when $T=0$, $r_1(t)\sim t^{-1/2}$, and all the fjords have a fixed, but arbitrary width $\sim\pi|A(t)|r(t)$, dependent on the initial condition. It should also be stressed that these (exact) solutions are not self-similar.

For any positive value of T, the evolution equations become

$$\dot{a}\sim\frac{Q}{2\pi}\frac{1}{a}+\frac{T\alpha_0}{a^2r}, \tag{41}$$

$$\dot{r}\sim-\frac{Q}{2\pi}\frac{r}{|A|^2}+\frac{2T(\alpha_z+2\alpha_p)}{|A|^3r^2}, \tag{42}$$

$$\dot{\rho}\sim-\frac{Q}{2\pi}\frac{\rho}{|A|^2r}+\frac{T\alpha_p}{|A|^3r^2}. \tag{43}$$

Assuming $1/ar=O(1)$ when $t\to+\infty$, we get from Eq. (41) that $a\sim a_0\sqrt{t}$, thus $|A|\sim A_0\sqrt{t}$ with $A_0=\sqrt{Q/\pi}$ and the behavior of A is significantly the same as with $T=0$.

The behavior of the right-hand side of Eq. (42) as $t\to+\infty$ results from the balance of two opposing terms. The first, independent of T, term is dominant for the large values of r, whereas when r becomes small, the second T-dependent term becomes dominant. The solution of Eq. (42) is

$$r^3\sim\left(\frac{6T(\alpha_z+2\alpha_p)}{A_0^3}t+C_1\right)t^{-3/2}, \tag{44}$$

where C_1 is a constant of the integration. Equation (42) is a typical example of singularly perturbed system: for any small value of T, the perturbative term becomes eventually dominant. We conclude that $r(t)\sim r_{1,0}t^{-1/6}$, where the constant $r_{1,0}$ depends on T and on the symmetry, but is independent of the initial condition. Therefore, in the present context, the selection of a particular solution implies the existence of a stable fixed point for the variable $\tilde{r}_1(t)=|A(t)|^{1/3}r_1(t)$, to which all the solutions are attracted. An illustration of this behavior is given in Fig. 5, where $r(t)$ has been plotted as a function of t for different initial conditions, both with $T>0$ and $T=0$.

Let us note that this method [21] of explaining selection in viscous fingering is completely independent of previous approaches and yields a new argument in favor of the microscopic mechanism hypothesis [22].

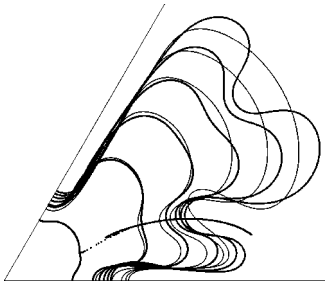

FIG. 6. A comparison between the interface obtained by a pseudospectral code (thick line) [20] and the approximation by the two-singularity model (thin line). The middle point of the fjord entrance, as computed with the second of these methods, is also represented.

The evolution equation (43) for ρ can also be integrated and shows a similar behavior. We have

$$\rho\sim[C_2+R(t)]\exp\left(-\frac{6Qt^{1/6}}{2\pi A_0^2r_0}\right), \tag{45}$$

where C_2 is a constant with respect to t and $R(t)$ reads

$$R(t)=\frac{T\alpha_p}{A_0^3r_0^2}\int_1^t x^{-7/6}\exp\left(\frac{6Qx^{1/6}}{2\pi A_0^2r_0}\right)dx. \tag{46}$$

As for r, the surface tension changes drastically the evolution of ρ when $t\to+\infty$. It can be shown (with two integrations by parts, for instance) that the leading term is

$$\rho\sim\frac{2\pi}{Q}\frac{T\alpha_p}{A_0r_0}t^{-1/3}. \tag{47}$$

V. SYMMETRIC SOLUTIONS WITH TWO SINGULARITIES

We now turn to the study of symmetric solutions with two singularities. This corresponds to the study of the first tip-splitting in the wedge experiments of Couder [8]: the primary singularities form the fjords parallel to the walls of the wedge-shaped cell and the secondary singularities will form the tip-splitting. According to their experimental observations, it should be expected that the fjords formed in this process are curved when the secondary singularities are far from the bisector. Figure 6 shows a typical example of how the two-singularity model approaches curved fjords. In this figure, we compare the interface evolutions obtained by our model and by a pseudospectral code [20]. The same initial condition has been used in both cases. The first tip-splitting gives a secondary curved fjord, which is approached by a straight fjord that changes its orientation in such a way that the middle point of its entrance describes accurately the curved fjord. The last tip-splitting observed in this figure cannot be accounted for by the two-singularity models, by definition.

The aim of this section is a complete description of the dynamics generated by the interaction between primary and secondary singularities. To achieve this goal, several approaches are possible. In Ref. [21], we considered a repre-

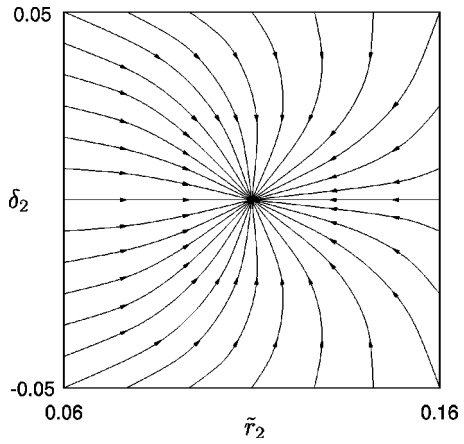

FIG. 7. Phase portrait in the $(\tilde{r}_2,\delta_2)$ space, obtained with ρ_2 and φ_2 fixed, $s=4$. All the trajectories converge towards a fixed point located in the vicinity of $(0.11,0)$.

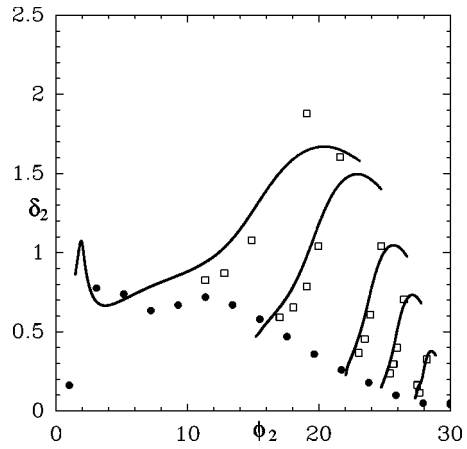

FIG. 8. Plot of the predicted asymptotic values $\delta_{2,0}$ of δ_2 as a function of ϕ_2 for a series of independent simulations, $s=6$. Continuous line: nonasymptotic values obtained in the simulation with two couples of singularities. See text for further details.

sentative set of particular solutions of the two-singularity model, and concluded the existence of a bifurcation as s goes from 4 to 6. Although informative, this approach does not really explain how this bifurcation occurs as, for instance, there is no indication about the existence of unstable fixed points. Here, we adopt a different strategy and draw the phase portrait as given by the Padé approximation (21). As a first approximation, the primary singularities will be considered as fixed (this approximation was not used in Fig. 6). This is certainly reasonable provided the primary and secondary singularities are well separated angularly, but becomes problematic as soon as they get close. Still, we are left with a set of four real coupled equations that govern the evolution of z_2 and p_2. In order to proceed further, we need to eliminate ''irrelevant'' degrees of freedom. A possibility, inspired by the notion of stable manifold [23], is to look for attracting sets in the space $(r_2,\rho_2,\theta_2,\phi_2)$. If those exist, it is possible to study the dynamics constrained to any of these sets, which amounts to an effective reduction of degrees of freedom. By analogy with the situation encountered in the study of the primary fjords, it should be expected that the width of the secondary fjords is selected with a value presumably dependent on the relative position of its closest neighbors. Inspired by the ''normal rule'' [8], it should also be expected that the orientation of the fjord is not arbitrary, but depends on ϕ_2. The width and orientation of the fjord associated with the couple (z_2,p_2) are given by the module and phase of c_2 which asymptotically behaves as $-Ae^{-i\phi_2}[r_2+i(\theta_2-\phi_2)]$. Therefore, we expect that, for each set of values of z_1,p_1,ρ_2,ϕ_2, there exist stable fixed points for r_2 and $\phi_2-\theta_2$, to which the solutions are attracted. This indeed is the case, as can be seen in Fig. 7. Before drawing the reduced phase portrait, it is useful to make time independent the attracting sets. We have found it convenient to look for fixed points $\tilde{r}_{2,0}$ and $\delta_{2,0}$ of the rescaled variables $\tilde{r}_2=|A|^{1/3}r_2$ and $\delta_2=|A|^{1/3}(\theta_2-\phi_2)$. From a numerical point view, the fixed points are found by iterating a Runge-Kutta algorithm until the time derivatives $\dot{\tilde{r}}_2$ and $\dot{\delta}_2$ are smaller than some threshold.

Properly speaking, the method to eliminate $\tilde{r}_2$ and δ_2 is not an adiabatic reduction, in the sense that there are not two different time scales in Eq. (21). In this sense, the method is expected to be accurate only asymptotically. In order to test this point, we run a set of simulations in which, for $s=6$, the initial angular position of the secondary singularity is varied. $\tilde{r}_{2,0}$ and $\delta_{2,0}$ can be computed (Figs. 8 and 9) either by using (z_1,p_1) as given by the selected one-singularity solution (dots) in which case z_1 and p_1 are mostly constant or as given by the computed two-singularity solution (open squares). In the second case, (z_1,p_1) can significantly differ from the one-singularity solution. In Figs. 8 and 9 are also shown the actual (nonasymptotic) values taken by δ_2 and r_2. These data give support to the claim that the asymptotic behavior of $\tilde{r}_2$ and δ_2 is governed by the position of the fixed points $\tilde{r}_{2,0}$ and $\delta_{2,0}$.

The asymptotic phase portrait as reduced to the manifold $\tilde{r}_2=\tilde{r}_{2,0}(\rho_2,\phi_2),\delta_2=\delta_{2,0}(\rho_2,\phi_2)$ for $s=4$ and $s=6$ can

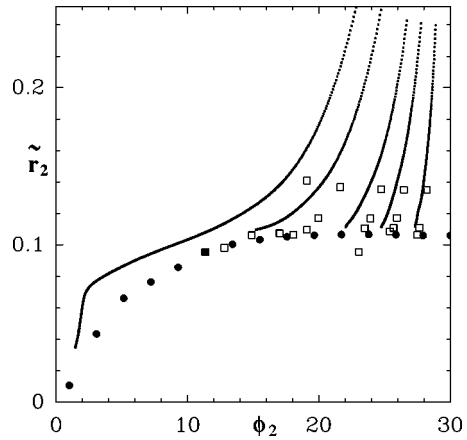

FIG. 9. Plot of the predicted asymptotic values $\tilde{r}_{2,0}$ of $\tilde{r}_2$ as a function of ϕ_2 for a series of independent simulations, $s=6$. Continuous line: nonasymptotic values obtained in the simulation with two couples of singularities. See text for further details.

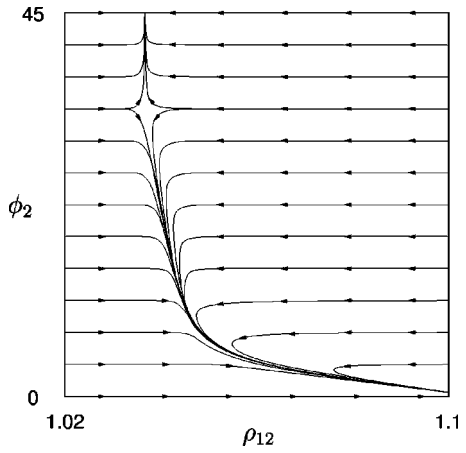

FIG. 10. Reduced vector field describing the dynamics of (ρ_{12},ϕ_2), $s=4$.

now be computed. In order to obtain a time independent phase portrait, we use $\rho_{12}\equiv\ln\rho_1/\ln\rho_2$ instead of the variable ρ_2. The corresponding phase portraits for $s=4$ and $s=6$ are shown in Figs. 10 and 11. The differences between the two are striking. For $s=4$, a fixed saddle point exists ($\phi_2\sim 40°, \rho_{12}\sim 1.02$), splitting the phase space into two regions: (i) the basin of attraction of the symmetric tip-splitting and (ii) all the solutions that are eventually attracted to $\phi_2=0$. When $s=6$, the first region disappears, as the fixed point becomes unstable in the two directions. The asymptotic behavior of the $\phi_2\to 0$ solutions is also different in the two cases. When $s=4$, ρ_{12} grows without limit as $\phi_2\to 0$, and $p_2\sim z_1$, which implies that (z_2,p_2) gets very close to the principal singularities and simply corrects the singularity structure of the primary fjord. Therefore, in this case, there is no formation of a secondary fjord. According to Tanveer's theory [10], a singularity with a $-4/3$ exponent is expected rather than a simple pole or even a collection of poles, as is the case in the model. It should be expected that the corrections to the singularity structure provided by the second couple (z_2,p_2) are such that, locally, the interface is closer to that given by a $-4/3$ singularity. This remains to be proven.

On the other hand, when $s=6$, ρ_{12} stays bounded. This

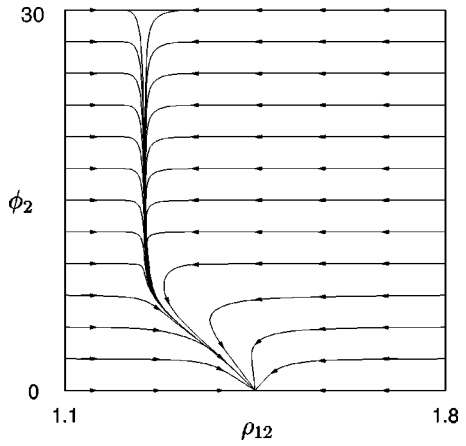

FIG. 11. Reduced vector field describing the dynamics of (ρ_{12},ϕ_2), $s=6$.

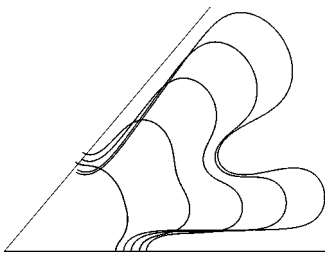

FIG. 12. Example of the solutions obtained with two couples of principal singularities, separated by an angle of 50°, interacting with a third couple that leads to the tip-splitting.

corresponds to the formation of a secondary fjord in one side of the main finger.

VI. NONSYMMETRIC TWO-SINGULARITY SOLUTIONS

In the Introduction of this paper, we mentioned the experimental findings of Lajeunesse and Couder [8] about the existence of a critical angle θ_c such that for wedge angles $\theta_0<\theta_c$, the symmetric tip-splitting is unstable. The results presented in the preceding section show that $90°\geqslant\theta_c\geqslant 60°$. To get a more precise value of θ_c, we need to relax the symmetry constraints. For this, we considered $s=2$ singularity configurations with *two* couples of principal singularities, angularly separated by an arbitrary θ_0. This reasonably approaches a wedge geometry with apex angle θ_0, as can be seen in Fig. 12. However, it is worth stressing that the asymptotic value of θ_0 is not necessarily that given as the initial condition. This is due to the delicate balance between the principal-principal and principal-secondary singularity interactions. This also reflects the fact that the singularity dynamics in a wedge is certainly simpler than that in an open geometry. For each of the values of θ_0 reported in Fig. 13, which correspond to the asymptotic value of the angular separation between the principal singularities, we computed the reduced phase portrait as explained in the preceding section. The angular position of the saddle point has been reported in Fig. 13. The fact that $(\theta_0/2-\theta_{\text{saddle}})^2$ behaves linearly as a function of $\theta_0-60°$ supports the claim that the saddle point arises from a pitchfork bifurcation [23] at

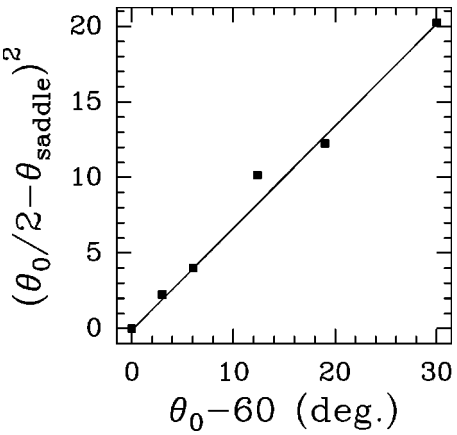

FIG. 13. Plot of $(\theta_0/2-\theta_{\text{saddle}})^2$ as a function of $\theta_0-60°$.

$\theta_0 = 60° = \theta_c$. This is compatible with the experimental observations of Lajeunesse and Couder [8,24].

VII. CONCLUSIONS

In this paper, we have studied a model for the growth of the interface separating two immiscible fluids in a Hele-Shaw cell. The model is based on the assumption that the shape of the fjords that form on the interface is logarithmic. This appears to be a rather natural assumption when viewed as a Padé approximation to the conformal mapping of the interface. One advantage of the model is that it becomes exact for zero surface tension, and yields explicit dynamical equations otherwise. The study of the latter shows that previous results concerning the existence of selection rules actually boil down to the existence of fixed points for the dynamics of certain variables. Moreover, the same argument can be extended to more complex situations, where primary and secondary fjords interact. In particular, we have shown that it is possible to derive selection rules for the width and orientation of the secondary fjords, in agreement with the experimental observations of Lajeunesse and Couder [8]. However, it is still unclear why the additional singularities that correct the logarithmic shape imposed in the present model do actually arrange in such a way that the middle line of the fjord follows what we have called the ''normal rule.'' Our analysis yields also a critical angle $\theta_c = 60°$, and $\beta = 0.40$ [25], which implies $D_f = 1.86$ using the approximations in Ref. [3]. We leave as an open question whether the above considerations can be generalized to more general situations. In the simplest mean field model studied so far, such as that in Ref. [3], it is assumed that the selection rules derived at the beginning of the growth can be applied in the subsequent stages of the growth. This is not obvious from the form of the coupling between different singularities, which decays fairly slowly [as $1/(z-z')^3$]. A somewhat unexpected consequence is that the random appearance of the tip-splitting phenomenon actually boils down to a slow ($\sim Tt^{-1/6}$) convergence to a limited number of fixed points: $\phi_2 = 0°$ when $\theta_0 < 60°$, $\phi_2 = 0°$ or $\phi_2 = \theta_0/2$ otherwise. In other words, the apparent dependence on initial conditions in viscous fingering is quite different from that of classical finite-dimensional chaos. The picture suggested here is rather that of a dynamical system with an infinite number of saddle points that are explored successively as the singularities approach the unit circle.

ACKNOWLEDGMENTS

All the simulations presented in this paper were done using the computer resources of the pôle M3PEC, Bordeaux 1 University. The authors acknowledge stimulating discussions with A. Sebbar, A. Arneodo, Y. Couder, and M. Ben Amar.

[1] D. Bensimon, L.P. Kadanoff, S. Liang, B.I. Shraiman, and C. Tang, Rev. Mod. Phys. **58**, 977 (1986).
[2] P. Pelcé, *Dynamics of Curved Fronts* (Academic Press, New York, 1988); D.A. Kessler, J. Koplik, and H. Levine, Adv. Phys. **35**, 255 (1988).
[3] S.K. Sarkar, Phys. Rev. Lett. **65**, 2680 (1990).
[4] D.A. Kessler, Z. Olami, J. Oz, I. Procaccia, E. Somfai, and L.M. Sander, Phys. Rev. E **57**, 6913 (1998).
[5] R.C. Ball, Physica A **140**, 62 (1986).
[6] L. Turkevich and H. Scher, Phys. Rev. Lett. **55**, 1026 (1985).
[7] F. Barra, B. Davidovitch, A. Levermann, and I. Procaccia, Phys. Rev. Lett. **87**, 134501 (2001).
[8] E. Lajeunesse and Y. Couder, J. Fluid Mech. **419**, 125 (2000).
[9] R. Combescot and M. Ben Amar, Phys. Rev. Lett. **67**, 453 (1991).
[10] S. Tanveer, Philos. Trans. R. Soc. London, Ser. A **343**, 1 (1993).
[11] M. Siegel and S. Tanveer, Phys. Rev. Lett. **76**, 419 (1996).
[12] M. Mineev-Weinstein, Phys. Rev. Lett. **81**, 5952 (1998).
[13] M. Ben Amar, Phys. Rev. A **43**, 5724 (1991).
[14] A. Arneodo, F. Argoul, E. Bacry, J.-F. Muzy, and M. Tabard, Phys. Rev. Lett. **68**, 3456 (1992).
[15] J. Elezgaray, Phys. Rev. E **57**, 6884 (1998).
[16] P. Henrici, *Applied and Computational Complex Analysis* (Wiley, New York, 1993), Vol. 3.
[17] S.D. Howison, J. Fluid Mech. **167**, 439 (1986); SIAM (Soc. Ind. Appl. Math.) J. Appl. Math. **460**, 20 (1986).
[18] M. Mineev-Weinstein and R. Mainier Phys. Rev. Lett. **72**, 880 (1994).
[19] C. M. Bender and S. A. Orszag, *Advanced Mathematical Methods for Scientists and Engineers* McGraw-Hill, New York, (1987).
[20] T. Hou, J. Lowengrub, and M. Shelley, J. Comput. Phys. **114**, 312 (1994).
[21] A. Pereira and J. Elezgaray, Europhys. Lett. **60**, 552 (2002).
[22] D.A. Kessler and H. Levine, Phys. Rev. Lett. **86**, 4532 (2001).
[23] J. Guckenheimer and P. Holmes, *Nonlinear Oscillations, Dynamical Systems and Bifurcations of Vector Fields* (Springer-Verlag, Berlin, 1983).
[24] Y. Couder (private communication).
[25] This is derived from the value of $\tilde{r}_{2,0}$ when $\phi_2 = 30°$.